Acta Oceanol. Sin., 2022, Vol. 41, No. 11, P. 126–138
https://doi.org/10.1007/s13131-022-2107-0
http://www.aosocean.com
E-mail: ocean2@hyxb.org.cn

HY-1C Coastal Zone Imager observations of the suspended sediment content distribution details in the sea area near Hong Kong-Zhuhai-Macao Bridge in China

Lina Cai[1], Minrui Zhou[1], Xiaojun Yan[1], Jianqiang Liu[2]*, Qiyan Ji[1], Yuxiang Chen[3], Juncheng Zuo[4]

[1] Marine Science and Technology College, Zhejiang Ocean University, Zhoushan 316004, China

[2] Key Laboratory of Space Ocean Remote Sensing and Application, Ministry of Natural Resources, Beijing 100081, China

[3] South China Sea Fisheries Research Institute, Chinese Academy of Fishery Sciences, Guangzhou 510300, China

[4] College of Marine Sciences, Shanghai Ocean University, Shanghai 201306, China

Received 24 April 2022; accepted 6 June 2022

Abstract

The impacts of the Hong Kong-Zhuhai-Macao Bridge (HKZMB) on suspended sediment content (SSC) were analysed in the Zhujiang River Estuary based on data from HY-1C, which was launched in September 2018 in China, carrying Coastal Zone Imager (CZI) and Chinese Ocean Color and Temperature Scanner on it. A new SSC inversion model was established based on the relationship between *in-situ* SSC and the remote sensing reflectance in red and near-infrared bands of CZI image. HY-1C satellite data obtained from October to December 2019 were applied to retrieve SSC in the Zhujiang River Estuary. The results show that SSC around the HKZMB is ranging from 20 mg/L to 95 mg/L. SSC change obviously on two sides of the bridge. During flooding and ebbing period, SSC increases obviously downstream of the bridge. SSC difference between upstream and downstream is ranging from 5 mg/L to 20 mg/L. Currents flowing across the HKZMB, the change trend of SSC in most places upstream and downstream is almost the same that SSC downstream of the bridge is higher than SSC upstream. The tidal currents interact with bridge piers, inducing vortexes downstream, leading the sediment to re-suspend downstream of the bridge piers. Other factors, including seafloor topography and wind, can also contribute to the distribution of SSC in the Zhujiang River Estuary.

Key words: HY-1C Coastal Zone Imager (CZI), Hong Kong-Zhuhai-Macao Bridge, suspended sediment content, Zhujiang River Estuary

Citation: Cai Lina, Zhou Minrui, Yan Xiaojun, Liu Jianqiang, Ji Qiyan, Chen Yuxiang, Zuo Juncheng. 2022. HY-1C Coastal Zone Imager observations of the suspended sediment content distribution details in the sea area near Hong Kong-Zhuhai-Macao Bridge in China. Acta Oceanologica Sinica, 41(11): 126–138, doi: 10.1007/s13131-022-2107-0

1 Introduction

Suspended sediment, as one of the major elements of ocean colour, plays an important role in coastal environment by affecting the process of biology, physics and geochemistry. It has an influence on luminous flux in water which is a key point to primary productivity (Shi et al., 2017) and can influence morph dynamical evolution of estuaries by process of depositing, flocculating and settling (Elias et al., 2012). The suspended sediments can be transferred by ocean current and they were redistributed in coastal waters. Therefore, analysing the distribution of suspended sediments in coastal waters is of great significance to the coastal environmental management (Cai et al., 2020), and it is a key point for the impact of offshore engineering on the marine environment (Chen and Gu, 2000; Li et al., 2017).

Prior researchers have developed many methods to detect suspended sediment content (SSC) based on remote sensing technology. The key of obtaining a SSC inversion model is to find the relationship between the sensitivity of satellite remote sensing data and suspended sediments (Cai et al., 2015; Lodhi et al., 1998). The relationship between the spectral reflectance of laboratory water and the total suspended particulate matter content showed that there exist non-linear relationships, such as exponential relationship, logarithmic relationship, quadratic relationship, cubic (Zhu et al., 2015; Nanu and Robertson, 1990; Forget et al., 2001; Yang et al., 2003, 2013) between them. In addition, liner relationship (Cai et al., 2020; Yang et al., 2003) was also revealed. In different bands, the red band (Novo et al., 1991) and the near-infrared band (Gordon and Morel, 1983) have the highest correlation with SSC.

Many offshore engineering facilities, such as Hangzhou Bay

Foundation item: The Zhejiang Key Science and Technology Project under contract No. 2020C02004; the National Key Research and Development Program of China under contract Nos 2017YFA0604901 and 2017YFA0604902; the Basic Public Welfare Research Program of Zhejiang Province under contract No. LGF21D010004; the National Key Research and Development Program of China under contract No. 2016YFC1401605; the National Natural Science Foundation of China under contract No. 41776183; the Curriculum Ideological and Political Teaching Research Project in the Universities of Zhejiang Province (Grouped Ideological and Political Teaching Model Research in the Subject of Marine Remote Sensing).
*Corresponding author, E-mail: jqliu@mail.nsoas.org.cn

Bridge, airports in the Jinzhou Bay, and Ningbo North Dyke (Cai et al., 2019, 2020; Yan et al., 2015), have been built in coastal areas. These facilities have impacts on ocean dynamic environmental factors (Park and Park, 1998; Xu et al., 2004). The change of dynamical environmental factors will induce the change of phytoplankton, SSC (Yuan and Lu, 2001), and SST (Huang et al., 2020) in the ocean. Detection of the impact of coastal engineering on the ocean environment was difficult until the advent of satellite remote sensing technology. Prior researchers applied satellite data to detect the change of SSC induced by bridges and ports in coastal waters (Qiao et al., 2011; Feng et al., 2014; Dai et al., 2006) and found that these engineering have changed the distribution of SSC. For example, SSC change induced by Donghai Bridge was analysed using the Medium Resolution Imaging Spectrometer (MERIS) and Thematic Mapper (TM). SSC increased near the bridge and then decreased in the area 5 km away from the bridge downstream (Qiao et al., 2015). During the construction of the cross-sea bridge in the Jiaozhou Bay, the increased flow on the north side of the bridge brought coarser seabed sediments from north to south of the Jiaozhou Bay (Zhao et al., 2015). Furthermore, researchers revealed that the downstream SSC increased at 3.0–6.5 km away from the bridge when the upstream SSC was low in the Hangzhou Bay. However, when the upstream SSC was greater than 400 mg/L, SSC decreased downstream (Cai et al., 2019). Meanwhile, the impacts of small-scale coastal engineering on SSC based on remote sensing data have also been analysed (Cai et al., 2019). However, prior studies mainly focused on the influence of engineering on surrounding waters environment in high turbidity water. It is necessary to study the impacts of coastal constructions on surrounding ocean environmental factors in low turbidity water.

The HKZMB was completed and put into use in 2018, and its effect on the marine environment turbidity water of Zhujiang River Estuary is not clear. Studies of sediments containing metal contents in the Zhujiang River Estuary have been performed using satellite remote sensing data (Li et al., 2000, 2001). Based on long-term analysis of hydrological and meteorological data, some studies have found the decreased trend and annual cycle period (4–8 a) for sediment load in Zhujiang River Estuary (Dai et al., 2008; Wu et al., 2014). Many studies have focused on suspended sediments observation in the Zhujiang River Estuary, but few studies focus on the influence of the HKZMB on surrounding waters using HY-1C satellite observation.

HY-1C, launched in China in 2018 for ocean observations, is a new satellite carrying Coastal Zone Imager (CZI) and Chinese Ocean Colour and Temperature Scanner. HY-1C CZI has a high resolution of 50 m and a great potential for small-scale marine monitoring such as chlorophyll *a* concentration observation in the Bohai Sea (Chen et al., 2019) and SSC in the Hangzhou Bay (Cai et al., 2020). However, these studies mainly focus on high turbidity water. It is urgent to develop low turbidity water algorithm based on HY-1C for the Zhujiang River Estuary, and reveal SSC distribution details near the HKZMB in Zhuhai.

2 Data and methods

2.1 *Study area*

The Zhujiang River Estuary (22.25°–22.90°N, 113.4°–114.2°E) is a composite delta, consisting of the west, the north and the east river deltas, from which three rivers flow into the sea (Fig. 1). The Zhujiang River is the third-largest river in China and its discharge in the basin mainly depended on the amount of rainfall (Chen and Chen, 2008). The average annual total runoff from the Zhujiang River Mouth to the sea ranks second compared to the Changjiang River in China, at about 3.26 km^3, and the amount of sediment at the entrance is 70.98×10^6 t (Zu et al., 2014).

The Zhujiang River Estuary mainly includes three major estuaries of the Lingdingyang Bay, Modaomen Estuary, and Huangmao Bay (Fig. 1). Each estuary has different widths and topographic features (Wong et al., 2003). The Lingdingyang Bay is a wide, shallow water area, and the sediments are mainly trumpet-shaped and there are 350 islands of different sizes, such as Qi'ao Island and Neilingding Island. The average depth of the Zhujiang River Estuary is about 4.8 m, but it can reach 10–20 m in the west channel and the east channel. The flood season in the Zhujiang River Estuary is from May to October, and dry season is from November to next April. The Zhujiang River has a subtropical monsoon climate and the tide type is irregular semidiurnal tide (Wang et al., 2018).

The HKZMB (black line in Fig. 1b) is a mega-size cross-sea bridge linking Hong Kong, Zhuhai and Macao. It is located in the Lingdingyang Bay, which is an estuary with weak tide, and the tide type is irregular semidiurnal mixed tide. The HKZMB is the longest bridge-tunnel system sea-crossing bridge in the world, crossing the waters of the Lingdingyang Channel in the Zhujiang River Estuary. The bridge starts from the artificial island of the Hong Kong Port near the Hong Kong International Airport in the east, crosses the Lingdingyang waters of the South China Sea to the west, connects Zhuhai and Macao artificial islands, and ends at Zhuhai Hongwan Interchange. The bridges and tunnels are 55 km in length, including the 29.6-km-length in main bridge, and 41.6-km-length from Hong Kong Port to Zhuhai-Macao Port. The information of the HKZMB was shown in Table 1.

2.2 *Satellite data and data processing*

The data product of HY-1C satellite was provided by National Satellite Ocean Application Service, Ministry of Natural Resources of the People's Republic of China. Images of HY-1C CZI from October to December in 2019 were obtained from the National Satellite Ocean Application Service (https://osdds.nsoas.org.cn) in China. These images were obtained around 10:50 local time under clear sky condition. The preprocessing of CZI image and definition of products at all levels are as follows. The level 1A data are obtained from level 0 data after geometric correction, including the digital number values of blue, green, red, and near-infrared bands. After radiometric calibration and atmospheric correction, we got level 2A (L2A) data. Having been geometrically positioned and performed atmospheric correction, L2A CZI data can be applied to inverse the elements of ocean color. The detailed information of CZI images was shown in Table 2.

In this paper, values from the L2A remote sensing images of CZI were applied as the Rrc (sr^{-1}) of the four bands corrected for Rayleigh scattering. A new SSC estimation model was established based on *in-situ* SSC and CZI L2A in the Zhujiang River Estuary. All calculations were performed in the softwares Python3.7 and ENVI5.3.

2.3 *In-situ data and processing*

We conducted data sampling activities around 10:52 on 14 December 2019 in the Zhujiang River. The ship traveled along the Zhujiang River to the Zhujiang River Estuary, collected data every 500 m, and obtained water samples for SSC measurement. Totally, 15 fishing ships at different positions in the sampling area, their locations were changed and water samples were collected around 10:52. Satellite data was acquired at 10:52 providing satellite Rrc synchronously. The matchup analysis between

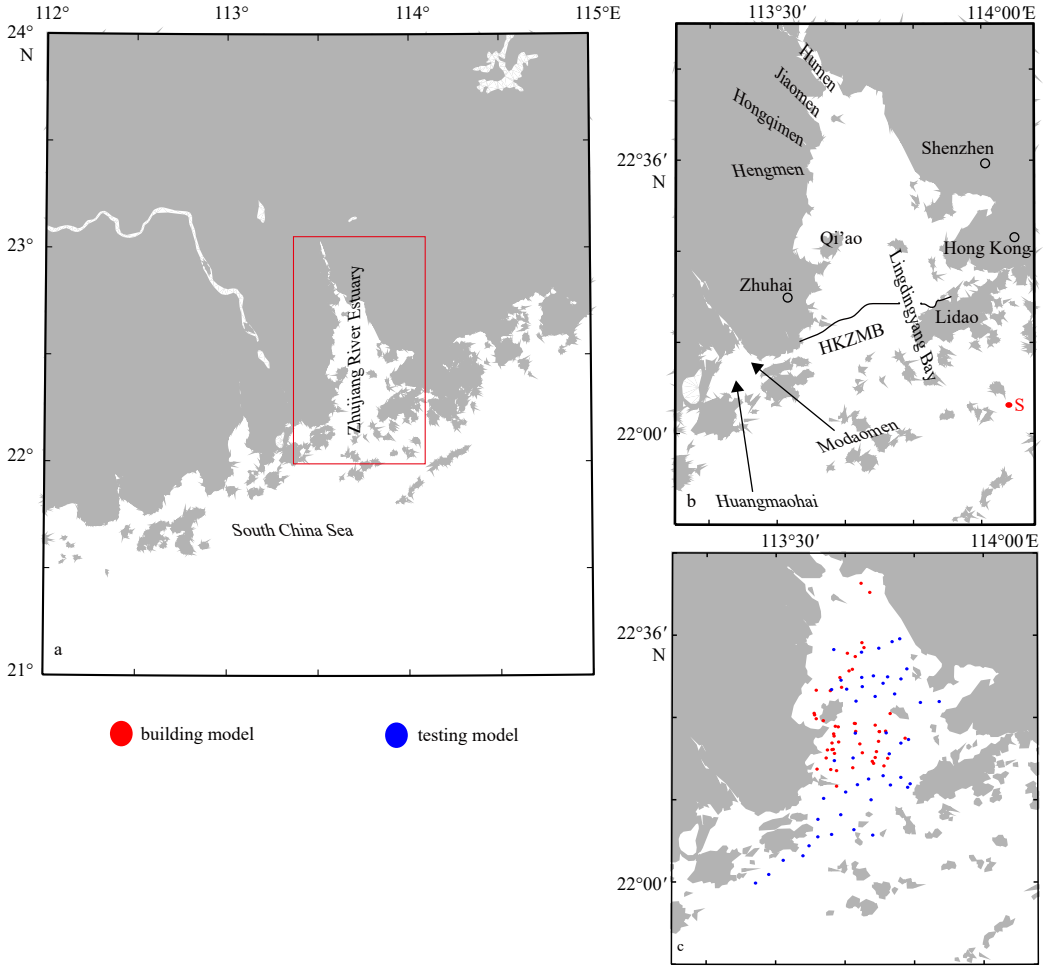

Fig. 1. Location of the Zhujiang River Estuary. Black line in b is the Hong Kong-Zhuhai-Macao Bridge (HKZMB). Station S marks the position of *in-situ* current measurement. The red points are sampling sites for building model and blue points are sampling sites for testing model.

Table 1. Information of the Hong Kong-Zhuhai-Macao Bridge

Length/km	Width/m	Starting date	Opening date	Number of piers	Distance between piers/m
55	33.1	November 15, 2009	October 24, 2018	224	85 (shallow), 110 (deep)

Table 2. HY-1C Coastal Zone Imager (CZI) sensor parameters and CZI data acquisition dates

Band	Rang/μm	Resolution/m	Application	Synchronous acquisition date of Bands 1, 2, 3 and 4
Band 1 (blue)	0.421–0.500	50	chlorophyll, pollution, sea ice, underwater topography	October 21, 2019; October 27, 2019; November 11, 2019; November 17, 2019; November 22, 2019; December 4, 2019; December 11, 2019; December 14, 2019; November 11, 2019; November 14, 2019; November 30, 2019; December 2, 2019; December 9, 2019; December 17, 2019; December 21, 2019
Band 2 (green)	0.517–0.598	50	chlorophyll, medium and low content sediment, pollution, vegetation, sea ice, tidal flat	
Band 3 (red)	0.608–0.690	50	medium content sediment, pollution, vegetation, soil	
Band 4 (near infrared)	0.761–0.891	50	vegetation, high content sediment, atmospheric correction	

satellite Rrc and *in-situ* SSC can be performed. We acquired 100 *in-situ* data, 50 of them were used to build the inversion formula, and the left were for verifying the retrieved results. These sampling points evenly distributed in the areas of Zhujiang River Estuary with different SSC and different depth (Fig. 1c). On average, the resolution of the sampling sites is one effective sampling site per ten or fifteen square kilometers in study area. In addition, to find out the sensitive bands of SSC, we also selected 50 samples randomly in 100 *in-situ* values to analyze the correlation between Rrc (sr^{-1}) of each band and SSC.

SSC means the per unit volume of particulate matter. We first filtered the water samples, then dried the filters for 24 h at 40°C and reweighed for obtaining SSC value (Qiu, 2013).

The tidal current velocity and direction of study area from 8:00 on June 7 to 8:00 on June 8, 2020 were measured using a flow profilometer named FlowQuest_ADCP 600 to analyze the changing regularity of tidal current velocity and flow direction. FlowQuest_ADCP 600 can measure the speed and direction of water

flow in oceans, harbors, estuaries, lakes and rivers. It can measure effectively over long distance and withstand the pressure of deep water. The operating frequency of the ADCP is 600 kHz. Once mounted alongside the ship vertically, the instrument is about a meter underwater, and it can record a set of data every five seconds.

2.4 *Current data*

Tidal currents in the Zhujiang River Estuary can transport suspended sediments, influencing the distribution of SSC. Therefore, the tidal current information in the Zhujiang River Estuary is necessary for analyzing the distribution of SSC there. The tidal currents in study area have been predicted by an unstructured grid, finite-volume, primitive equation community ocean model (FVCOM) (Chen et al., 2006). FVCOM is well suited for the Zhujiang River Estuary, where is characterized by irregular complex coastlines, islands, and inter-tidal zones. The ocean model is forced by the tidal elevation and transport derived from eight tidal constituents (K_1, O_1, P_1, Q_1, K_2, M_2, N_2 and S_2). The tidal parameters come from the Oregon State University (OSU) global tidal data-base (Egbert et al., 1994; Egbert and Erofeeva, 2002; Chen et al., 2016). The numerical model has been validated in a prior study (Chen et al., 2016).

3 Results

3.1 *Current in study area*

The tidal type of the Zhujiang River Estuary is irregular semidiurnal tide. Take the current of the Zhujiang River Estuary on December 14, 2019 as an example (Fig. 2). During the ebbing period, the water flows southward from the tributaries and enters the South China Sea through the Zhujiang River Estuary. The flow velocity increases at first and then decreases. The flow velocity is the highest near Hong Kong Island. During the flooding period, the tidal current from the South China Sea poured into the Zhujiang River Estuary. The tide continued to rise until 12:00 noon (Fig. 2d), and the flow velocity decreased. Then ebb occurred again at 16:00 and flood at 20:00 in the evening. Characteristics of tidal current are regional. That is to say, the tidal type and characteristics of the same place are stable. We can apply the tidal pattern of an ordinary day as an example to illustrate this rule. In order to illustrate that the current velocity and direction

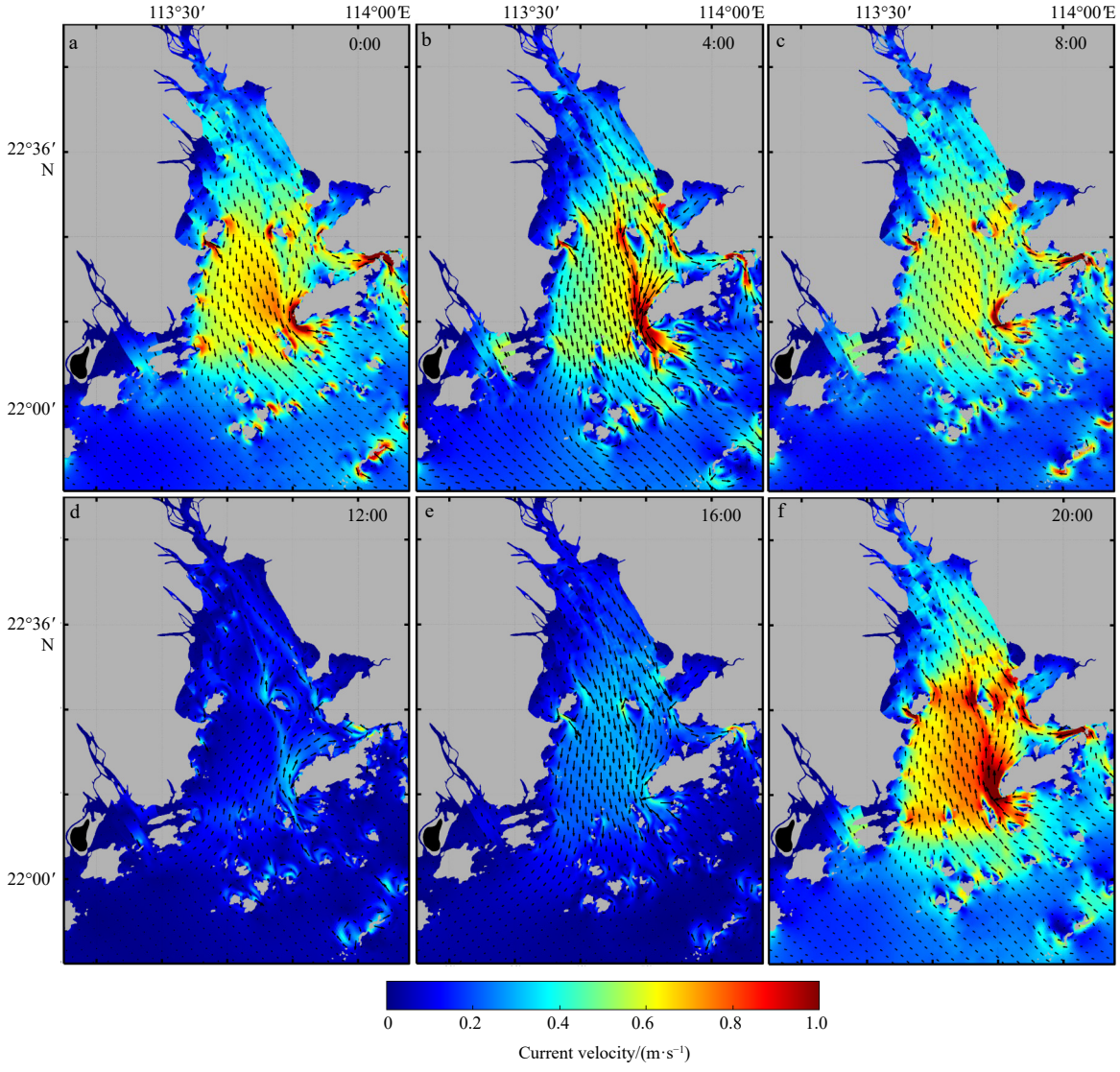

Fig. 2. The current velocity on December 14, 2019 in the Zhujiang River Estuary simulated by the unstructured grid, finite-volume, primitive equation community ocean model (FVCOM) model.

of tidal current in the study area are constantly changing with time further, we applied 24 h continuous observation of *in-situ* current velocity and direction to illustrate the change of tidal current velocity with time (Fig. 3). The observation of *in-situ* current velocity and direction during 24 h at Station S from 8:00 on June 7 to 8:00 on June 8, 2020 also showed that the velocity and direction of tidal current have changed with time (Fig. 3), taking on irregular semi-diurnal characters.

3.2 *Sensitive band of SSC*

The change of SSC can induce the change of reflectance value, as shown in the red band with the highest value of reflectance around 0.087. The lowest value of reflectance is about 0.005 when SSC is 12 mg/L. With the increase of SSC from 12 mg/L to 62 mg/L, the value of reflectance is also increasing and there appears a peak value in the green band. In the near-infrared band, there is no significant change in the value of reflectance. When SSC is up to more than 300 mg/L, two reflectance peaks (Fig. 4) appear in the *in-situ* measured reflectance curve, in the ranges of 550–600 nm and 630–700 nm. Therefore, it is obvious that when SSC is low, the green band and the red band are more sensitive to the reflectance of the sediments, while the red and the near-infrared band are sensitive to high SSC water.

The correlation between the Rrc (sr^{-1}) value of each band of CZI and the *in-situ* SSC was shown in Fig. 5. The coefficient of determination between the single band Rrc (sr^{-1}) and *in-situ* SSC is in the range of 0.004–0.67. The lowest value of R^2 is 0.003 9 for blue band (Fig. 5a) and the highest value is 0.665 3 for red band (Fig. 5c), indicating that the blue band is the least sensitive to the change of SSC, while the red band is the most sensitive to the change of SSC. The sensitivity of green band and near-infrared band to the change of SSC is stronger than blue band with the R^2 value of 0.166 7 (Fig. 5b) and 0.318 8 (Fig. 5d), respectively. According to the coefficient of determination values, the red band is most sensitive to the change of SSC, followed by the near-infrared band, and the sensitivity of the blue band and the green band to SSC is relatively weak (Fig. 5). Therefore, the Band 3 and the Band 4 of CZI were selected to build SSC inverse model.

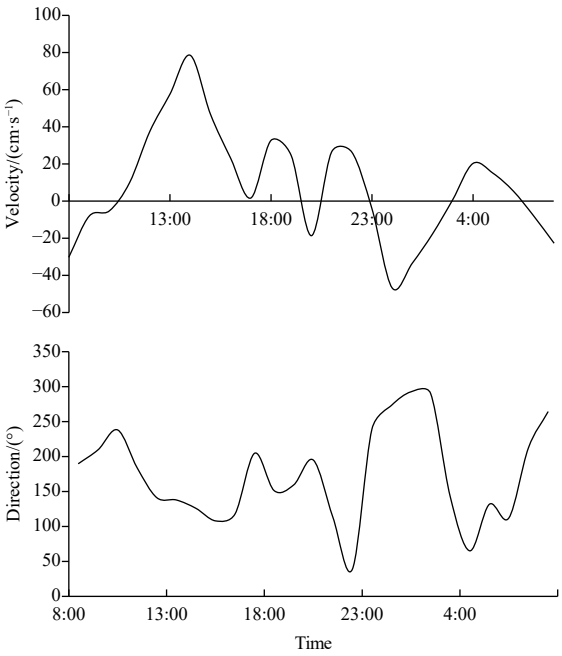

Fig. 3. Tidal current velocity and direction measurement at Station S (Fig. 1) during 24 h from 8:00 on June 7 to 8:00 on June 8, 2020. The angle calculation method takes north as 0° and increases clockwise: 90° for east, 180° for south and 270° for the west; the positive direction of the *y*-axis represents east and negative represents the west.

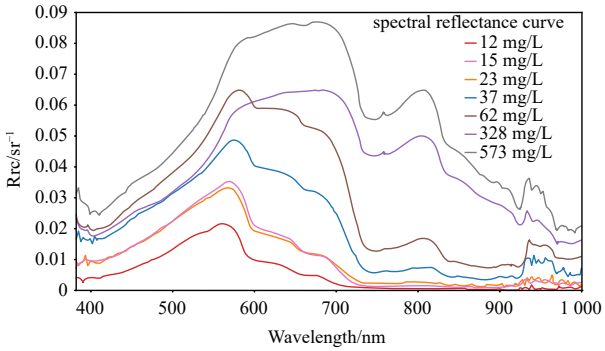

Fig. 4. Spectral reflectance curves of water with different suspended sediment content.

3.3 *A new SSC estimation model for HY-IC*

Based on the analysis of the water spectrum characteristics above, and combined with the band setting of the HY-1C satellite sensor and the response function of each band, the Band 3 and Band 4 were selected to build SSC inverse model (Table 3). The single band, band combination which is more sensitive to SSC was selected. The combination of Band 3 (red band) and Band 4 (near-infrared band) is sensitive to sediment concentration, as shown in Table 3 and we apply this combination to build SSC inversion model. Furthermore, previous studies have proved that the red and near-infrared bands combination method is more sensitive to changes of SSC (Wang et al., 2018).

Statistical regression remote sensing inversion models between single band or band combination and SSC in the water body were built and analyzed (Table 3). The winter voyage of the Zhujiang River Estuary has collected data from 100 points. To ensure the reliability of the model, half of the data was used for establishing the model and the remaining data was applied for verification. The model with the best stability and high accuracy will be applied to retrieve the distribution of SSC in the study area. The band combinations and the models were shown in Table 3.

Band combinations of B3 and B4 improve the fitting effect of the model, and the highest coefficient of determination can reach 0.981 2. Number 13 corresponds to the model with the highest correlation coefficient in Table 3.

$$\mathrm{SSC} = 7\,011.61 \times R_{\mathrm{red}} - 3\,386.62 \times R_{\mathrm{nir}}, \tag{1}$$

where SSC is the suspended sediment concentration (mg/L), R_{red} and R_{nir} are Rrc (sr^{-1}) of the third (red) and fourth (near-infrared) band after the atmospheric correction.

The model-estimated result shows a high consistency with *in-situ* SSC (RMSE is 3.07, R^2 is 0.93) (Fig. 6). It is obvious that the new built model is suitable for SSC inversion in the Zhujiang River Estuary. Furthermore, in prior study, it is valid for SSC retrieving at the Zhujiang River Estuary by using the reflectance at 645 nm (red band) and 825 nm (near-infrared band) (Zhang et al., 2010).

3.4 *SSC distribution in the Zhujiang River Estuary*

SSC in the Zhujiang River Estuary is ranging from 10 mg/L to

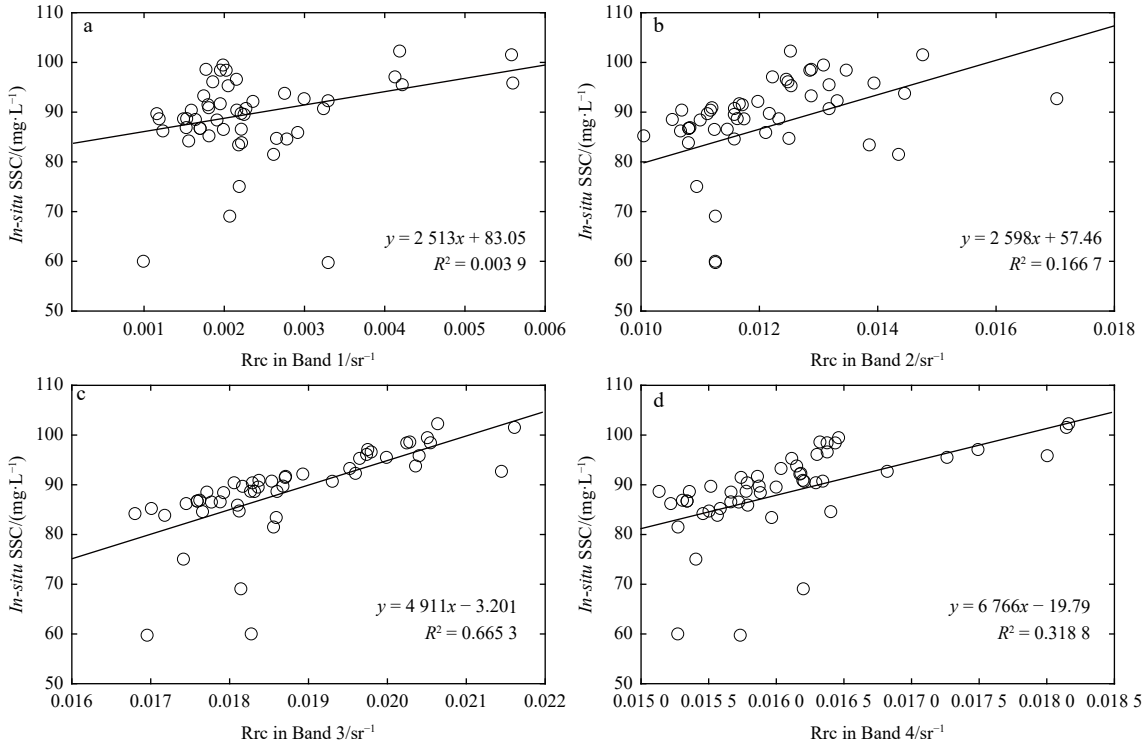

Fig. 5. Correlation between Rrc (sr^{-1}) of four bands and *in-situ* suspended sediment content (SSC).

Table 3. Summary of suspended sediment remote sensing inversion models in the Zhujiang River Estuary

Number	Band combination	Model	Correlation coefficient
1	B3	$5.02e^{104.3X}$	0.723 2
2	B3	$2\,686X - 15.3$	0.685 9
3	B3	$23\,120X^2 - 4\,517X + 39.95$	0.726 1
4	B3	$25\,660X^{1.656}$	0.704 5
5	B4	$4.825e^{155.6X}$	0.359 4
6	B4	$4\,695X - 24.39$	0.387 4
7	B4	$-801\,500X^2 + 25\,540X - 122.6$	0.411 5
8	B4	$90\,890X^{1.801}$	0.378 5
9	B4/B3	$472.1e^{-4.149X}$	0.641 9
10	B4/B3	$-96.2X + 94.22$	0.590 9
11	B4/B3	$552.2X^2 - 887.7X + 375.2$	0.675 2
12	B4/B3	$9.055X^{-2.096}$	0.655 6
13	B3, B4	$7\,011.61 \times B3 - 3\,386.62 \times B4$	0.981 2

Note: B3 is Rrc (sr^{-1}) in the third band (red band); B4 is Rrc (sr^{-1}) in the fourth band (near-infrared red band). *X* is the symbol of band combination.

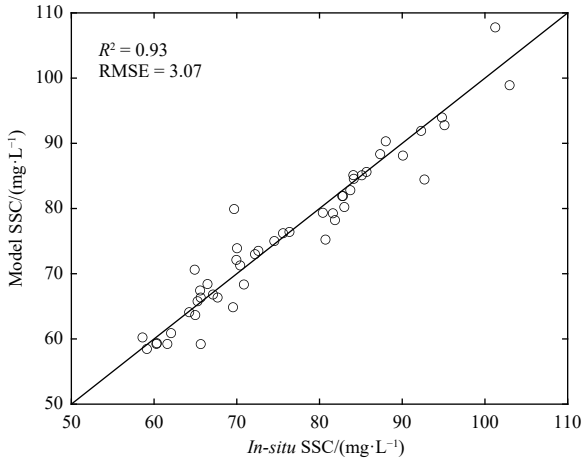

Fig. 6. Comparison of suspended sediment content (SSC) inversion value and *in-situ* SSC. RMSE: root mean squared error.

120 mg/L (Fig. 7) and is mainly lower than 100 mg/L. It is clear that SSC is higher in outlets of the west part than in the east part of the study area. SSC is high in the west and north parts of the Zhujiang River Estuary with SSC in the range of 80–120 mg/L. SSC in eastern coastal water near Hong Kong is the lowest, with SSC less than 40 mg/L. Among all the pictures in Fig. 7, SSC in the west shoal is the highest, and SSC in the middle shoal is lower than that of the west shoal.

3.5 *SSC distribution near the HKZMB*

SSC around the HKZMB is ranging from 20 mg/L to 120 mg/L (Fig. 8). It is clear that SSC upstream and downstream of the bridge is different, and the difference of SSC value is in the range of 5–20 mg/L.

The value changes suddenly at the position of the bridge because of the influence of the bridge. At a distance of 0.5 km from the upstream and downstream of the bridge, SSC value profiles of 7.5 km parallel to the bridge (Figs 8 and 9) were taken. Meanwhile, SSC profiles along the direction of current crossing the bridge were also analyzed (Fig. 10). The changing trend of SSC upstream and downstream of the bridge is stable.

During flooding and ebbing period, it is clearly SSC downstream the bridge is higher than SSC upstream the bridge (Fig. 9, Figs 10 a, b, e and f). The current flowing across the HKZMB, the change trend of SSC in most places upstream and downstream is almost the same, SSC increased obviously downstream of the bridge. The maximum difference in SSC from upstream to downstream is about 20 mg/L. Only a few places in Figs 10c and d showing reverse change. Generally, SSC downstream increased

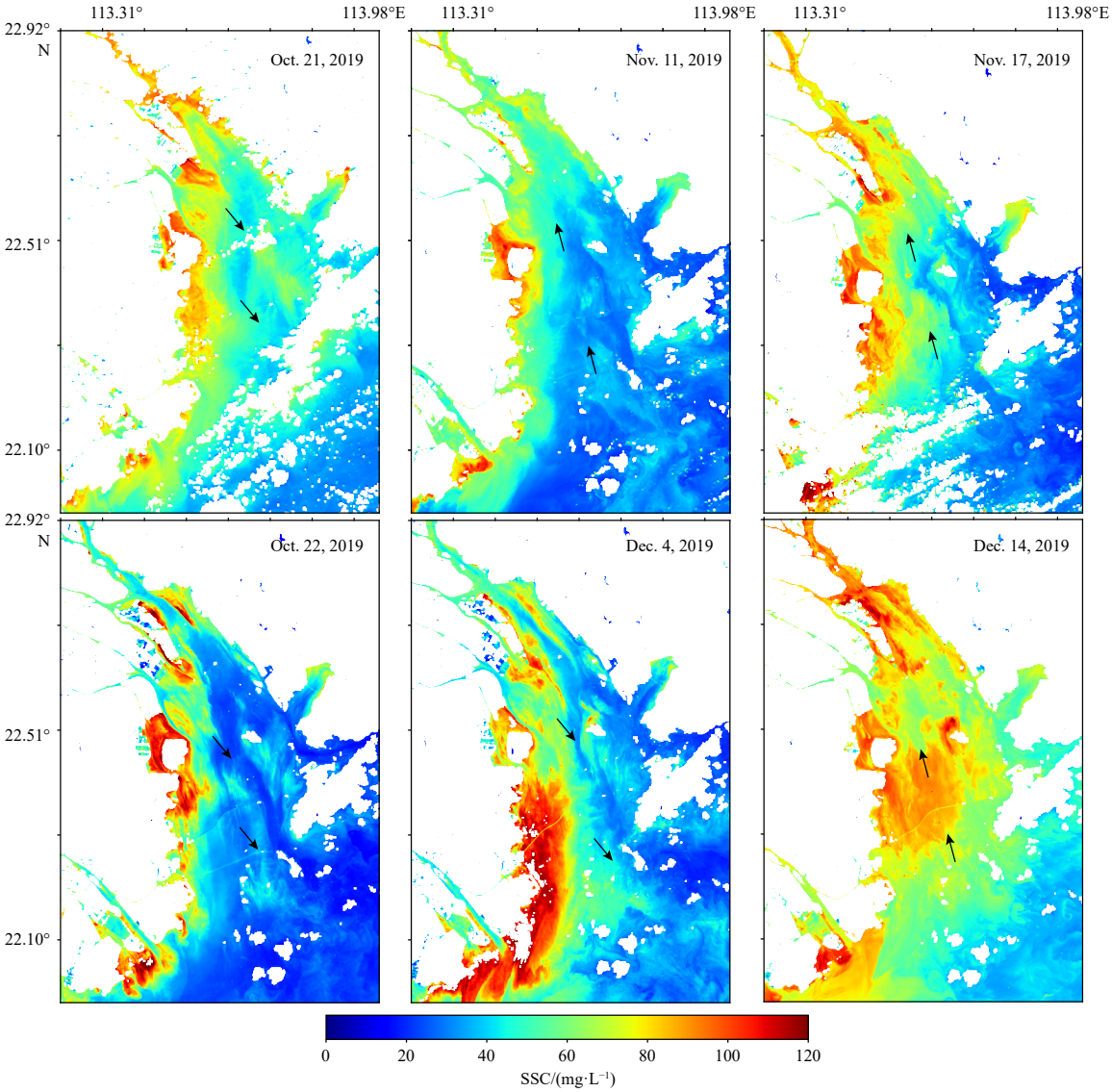

Fig. 7. The distribution of suspended sediment content (SSC) in the Zhujiang River Estuary retrieved from HY-1C Coastal Zone Imager images. Black arrow indicates the direction of local tidal current.

obviously and the maximum difference in SSC from upstream to downstream is about 20 mg/L. While, during plain tide and slack tide, SSC change from upstream to downstream is not obvious with SSC value almost the same in Fig. 9c. Meanwhile, SSC on two side of the bridge decreased gradually along the bridge from the west to the east.

4 Discussion

4.1 *Applicability of SSC inversion model for the Zhujiang River Estuary*

The correlation between the Rrc (sr^{-1}) value of each band of CZI and the *in-situ* SSC showed that the coefficient of determination between the Rrc (sr^{-1}) of single band and *in-situ* SSC is different in different bands. The highest value is 0.665 3 of the red band (Fig. 5c), indicating that the red band is the most sensitive band to the change of SSC. The sensitivity of the near-infrared band to the change of SSC is stronger than blue and green bands with the R^2 value of 0.318 8. According to the R^2 values, the red band is the most sensitive to the change of SSC, followed by the near-infrared band, therefore, the red band (Band 3) and near-infrared band (Band 4) of CZI are selected to build SSC inversion model. Many models have been developed to estimate SSC with empirical, semi-empirical, semi-analytical or analytical algorithms (Montanher et al., 2014; Wu et al., 2013; Zhang et al., 2014) based on satellite images, such as Moderate Resolution Imaging Spectroradiometer (Feng et al., 2014), MERIS (Loisel et al., 2014), and Landsat (Zhang et al., 2014) images. The near-infrared band and the red band appeared in most of these algorithms (Pope and Fry, 1997; Zhu et al., 2015). Our sensitive bands are consistent with prior studies (Pope and Fry, 1997; Zhu et al., 2015), which applied the red band and the near-infrared band to analyze SSC (Montanher et al., 2014; Wu et al., 2013; Zhang et al., 2014).

In total, water samples were collected from 100 sites, 50 of them were applied to establish SSC inversion model, and the other 50 values were used for calibration. These water samples evenly distributed in the Zhujiang River Estuary. The result estimated by the newly built model shows a high consistency with *in-situ* SSC (RMSE is 3.07, R^2 is 0.93) (Fig. 6). It is obvious that the newly built model is suitable to inverse SSC in the Zhujiang River Estuary. Zhujiang River Estuary is dominated by SSC lower than

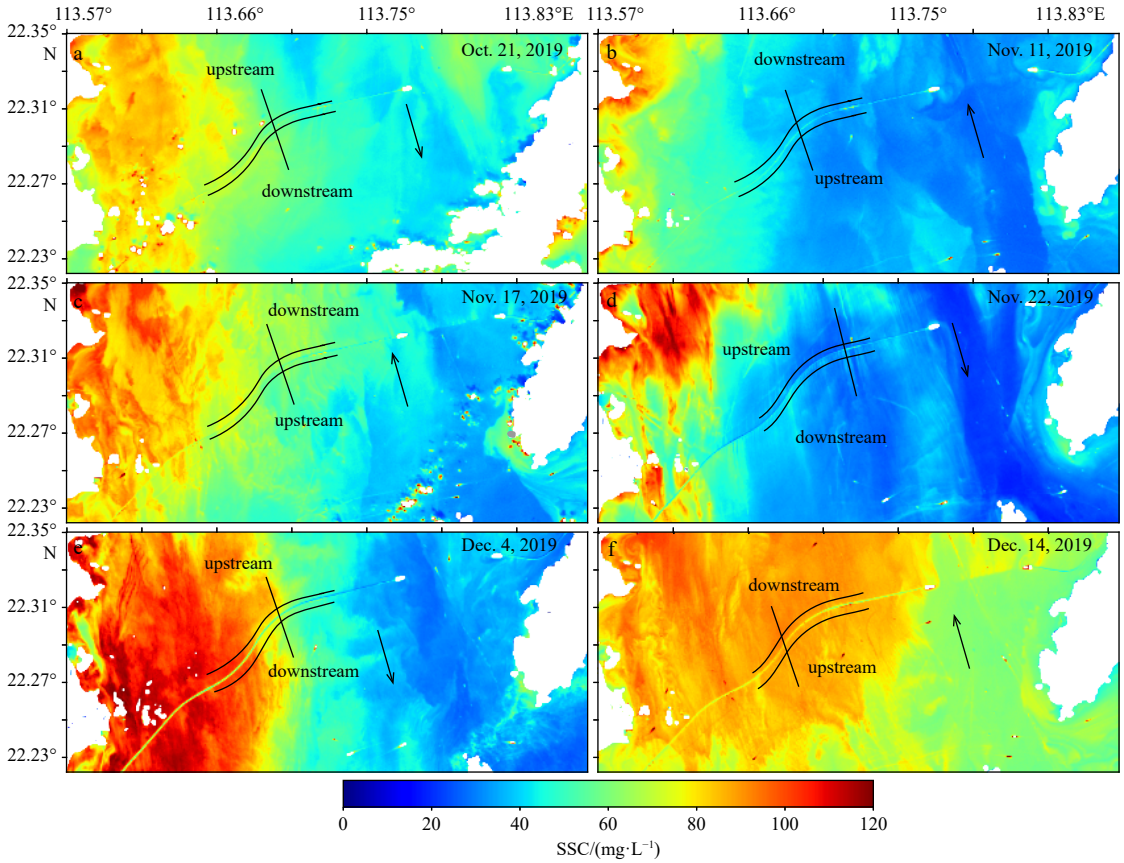

Fig. 8. The distribution of suspended sediment content (SSC) near the Hong Kong-Zhuhai-Macao Bridge retrieved from HY-1C Coastal Zone Imager images. Black lines mean SSC profiles sampled along the bridge and crossing the bridge.

100 mg/L. Generally, SSC is higher in outlets of the west part, with SSC in the range of 80–120 mg/L, than the east part of Zhujiang River Estuary where SSC is less than 40 mg/L. SSC in the west shoal is the highest and SSC in middle shoal was lower than that of the west shoal. The modeled SSC in the Zhujiang River Estuary obtained from CZI data is consistent with the results in prior studies (Dai et al., 2008; Wu et al., 2014) as well as *in-situ* SSC, with R^2 of 0.93.

SSC distribution detail near the HKZMB was revealed based on SSC obtained using the newly built model. SSC downstream of the HKZMB is higher than SSC upstream of the bridge (Fig. 9, Figs 10 a, b, e and f), no matter in the flooding period or in the ebbing period. SSC increased obviously downstream of the HKZMB, the maximum difference in SSC from upstream to downstream is about 20 mg/L. While, during plain tide and slack tide, SSC change from upstream to downstream is not obvious with SSC value almost the same (Fig. 9c). Meanwhile, SSC on two sides of the bridge decreased gradually along the bridge from the west to the east.

The sensors on CZI of HY-1C have four bands, including blue, green, red and near-infrared bands, and the spatial resolution is 50 m. In prior study, SSC in coastal zone obtained from CZI images has a good result (Cai et al., 2020), indicating its great potential for offshore observation.

4.2 *The natural factors influencing the distribution of SSC in Zhujiang River Estuary*

The spatial distribution of SSC in Zhujiang River Estuary is mainly influenced by the tidal currents, sea floor topography and wind. The fluctuation process of the tidal current directly affects the transport, settlement and re-suspension of suspended sediment, and thus influences the distribution of suspended sediment in the estuary (Xia et al., 2004). At the beginning and the middle stages of the flooding period, the low-sand water body of the continental shelf entered the Lingdingyang Bay, from the southeast along with the rising tide. The Lingdingyang Bay was wide and shallow. Under the influence of the ground transfer effect, the lateral tide is stronger than the west at the east part of the estuary. This makes the low-sand water body invade faster and farther to the east, and inhibits the transport of the high-sand water body at the entrance to the east, resulting in a flat distribution of low sand content in the east and low west (Fig. 11). During flooding period, high-sand water body in the west beach of the Lingdingyang Bay is partly covered by the rising tide and spreads like a tongue to the north side. During the ebbing period, the tidal current, together with the high SSC fresh water, flows out of the estuary bay toward the southeast, the high-sand water at the estuary gate and west side were transported by the tidal current (Liu and Cai, 2019; Wong et al., 2003).

Seasonal characteristics of SSC in the Zhujiang River Estuary is obvious (Wu et al., 2014). In winter, SSC is high at the western coast and the estuary of the Zhujiang River, while SSC in the southeast decrease gradually. SSC is lower in the open sea than it in other areas. This is mainly due to the influence of the northwestern winter monsoon and the runoff from the Zhujiang River. SSC is higher in the west coast than in the open sea in spring. There is a large runoff capacity during the summer and a flooding period, resulted that SSC in the west of the estuary is high. The runoff in autumn decreases, and the flush fresh water is weak, the high SSC only stays at the mouth of the Zhujiang River

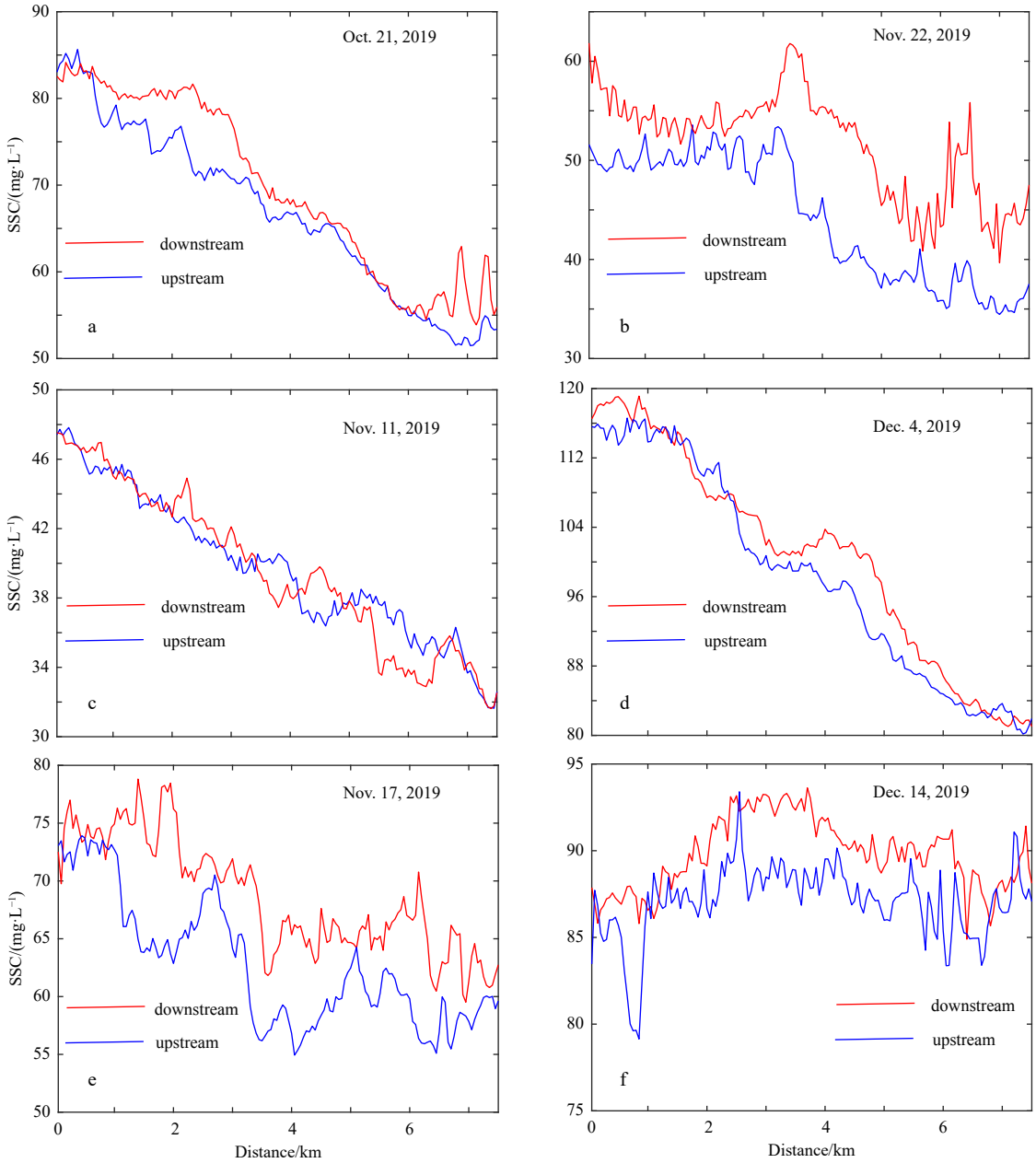

Fig. 9. Suspended sediment content (SSC) profiles sampled at 0.5 km away from the bridge's upstream and downstream. Blue line is SSC profile upstream; red line is SSC profile downstream.

and near the coast (Dai et al., 2008; Wang et al., 2018).

The Lingdingyang Bay is large, where wind waves penetrate in, especially when a typhoon surge occurs, inducing the sediments re-suspension in the western shoals of Lingdingyang Bay with tidal floods. The sediments can be carried by waves to the east and southeast, evenly exposed to the mouth of Zhujiang River Estuary (Graber et al., 1989; Liu and Cai, 2019).

Seafloor topography also plays an important role in influencing the distribution of SSC. SSC is higher (red circles in Fig. 11) in areas with shallow water, and SSC is low (blue circles in Fig. 11) in deep areas, which is consistent with prior studies (Cai et al., 2015).

4.3 *The influence of the HKZMB on SSC*

Human activities, such as the construction of dams and bridges (Yuan et al., 2009; Zhu et al., 2015), can also contribute to the distribution of SSC. The HKZMB has blocked the radial transport of suspended sediment in the Zhujiang River Estuary, resulting in obvious differences in the spatial distribution of suspended sediment on two sides of the bridge. In the high-concentration area of suspended sediment in the east of the Zhujiang River and near the east artificial island, the HKZMB has a significant impact on the spatial distribution of suspended sediment showing a phenomenon of SSC jump on two sides of the bridge (Fig. 7).

The HKZMB is 55 km long and has 224 piers (Table 1). The scouring of the bridge piers by the tidal current will affect the distribution of sediments. The tidal currents interact with bridge piers, inducing vortex wakes downstream (Umeda et al., 2010). Near the bridge piers, velocity of the current is the largest, forming vortexes downstream, causing the sediments to re-suspend downstream the bridge piers (Cai et al., 2015, 2020). When the

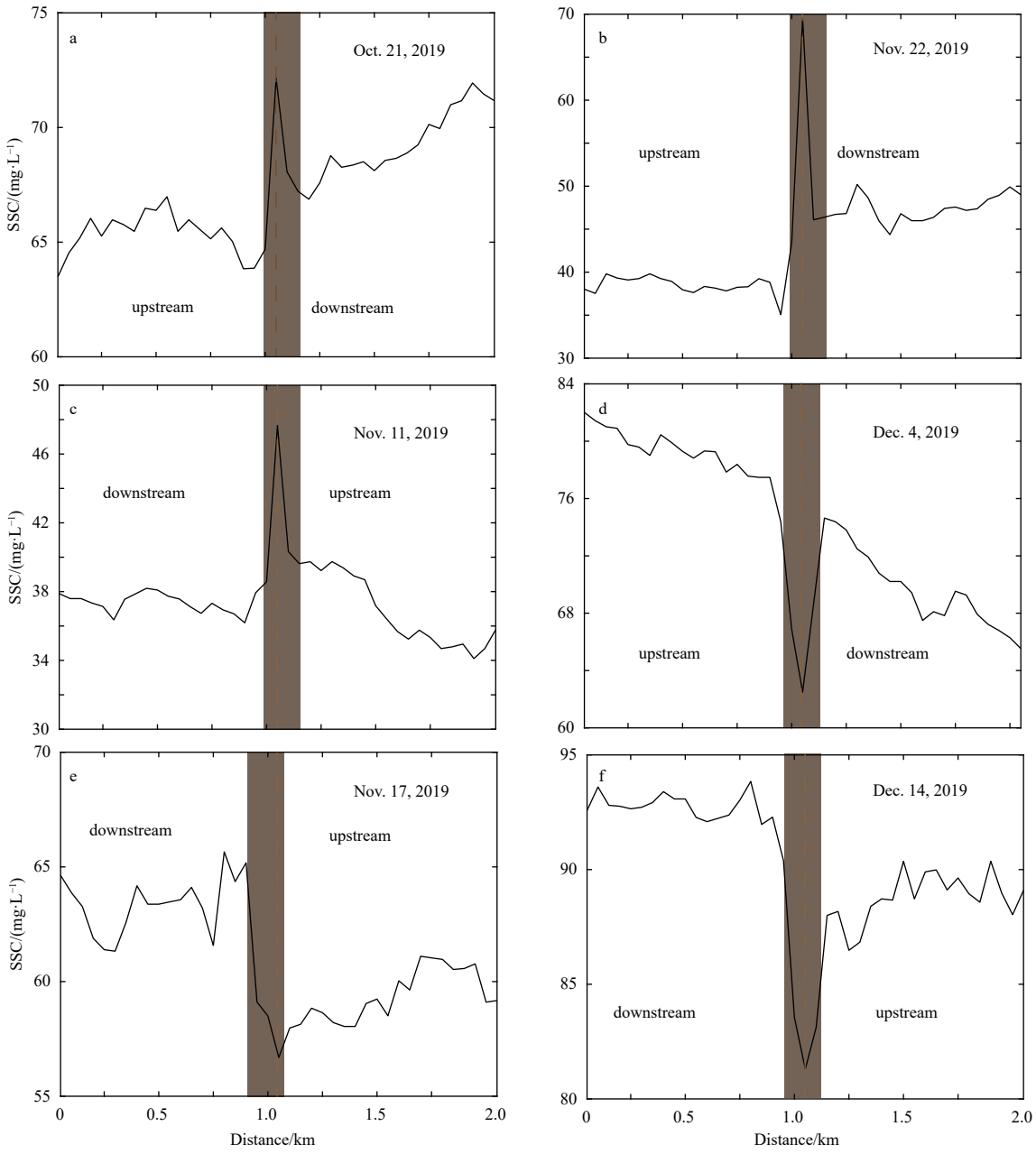

Fig. 10. Suspended sediment content (SSC) profiles sampled along the current crossing the Hong Kong-Zhuhai-Macao Bridge (HKZMB). The brown vertical pillar represents the HKZMB.

current shear stress is greater than the sediments initiation shear stress, resuspension of sediments around the piers will occur. Part of the sediments deposit downstream of the piers, and the other part will be carried away by the current (Yanmaz and Altinbilek, 1991), inducing higher SSC downstream of the bridge, as it was shown in Fig. 12.

Generally, in the water surrounding the HKZMB in the Zhujiang River Estuary, the distribution of SSC is influenced by the HKZMB significantly. The piers of the HKZMB interact with the currents, thereby inducing local scouring near the bridge and vortex streets downstream, resulting in sediment resuspension downstream and inducing the increase of SSC downstream accordingly. Before the presence of the HKZMB, with no piers interacting with the current, SSC there has no obvious difference.

5 Conclusions

This study analyzed the spatial variation of SSC in the Zhujiang River Estuary. The new HY-1C CZI satellite images can well inverse the distribution of SSC in the Zhujiang River Estuary. There was a significant spatial variation of SSC from 20 mg/L to 200 mg/L. SSC is higher in the outlets of tributaries than the southeast study area. SSC reaches the highest from tributaries outlets to Qi'ao Island. SSC in eastern coastal water of Lidao Island of Hong Kong is the lowest, with SSC less than 40 mg/L.

SSC around the HKZMB is ranging from 20 mg/L to 120 mg/L. SSC changes obviously on two sides of the bridge, showing a sudden increase or decrease in SSC, and SSC change on the upstream and downstream of the bridge is stable. SSC upstream and downstream of the bridge has the same change trend, i.e., SSC upstream of the bridge is lower than SSC downstream of the

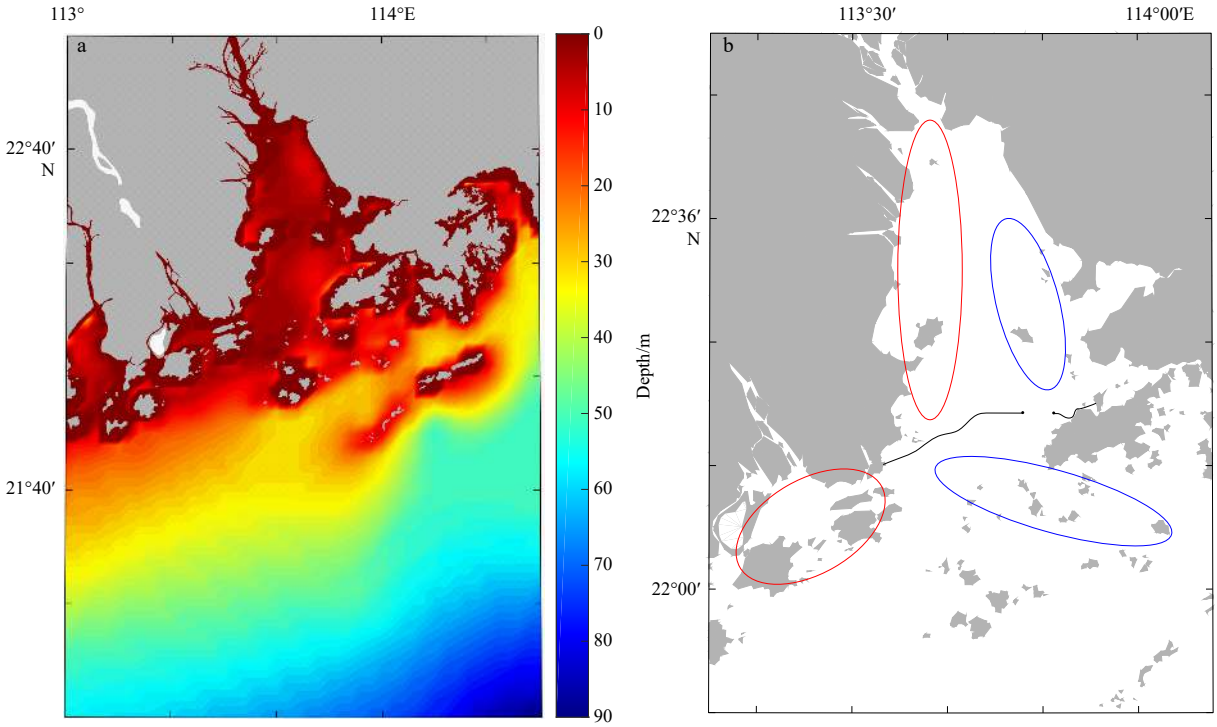

Fig. 11. The topography map (a) and average suspended sediment content (SSC) distribution (b) in the Zhujiang River Estuary. Red circles in b are high SSC area; blue circles in b are low SSC area.

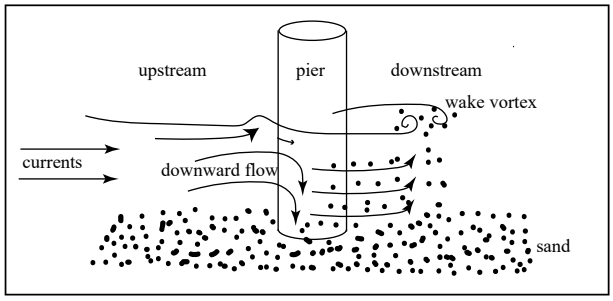

Fig. 12. Graphical abstract illustrates the impacts of bridge piers on the distribution of suspended sediment content (SSC). When currents pass through the piers of the Hong Kong-Zhuhai-Macao Bridge, the currents will scour the piers, leading a downward flow stirs the seabed of the Zhujiang River, and inducing wake vortex downstream of the piers. The interaction of current and the bridge piers will lead the sediments to re-suspend, inducing higher SSC downstream the bridge.

bridge at most of the time. The difference of SSC is ranging from 5 mg/L to 20 mg/L.

The tidal currents interact with bridge piers, inducing vortexes, leading the sediments to re-suspend downstream of the bridge piers (Fig. 12). Other factors, including sea floor topography and wind can also contribute to the distribution of SSC in the Zhujiang River Estuary.

References

Cai Lina, Tang Danling, Li Xiaofeng, et al. 2015. Remote sensing of spatial-temporal distribution of suspended sediment and analysis of related environmental factors in Hangzhou Bay, China. Remote Sensing Letters, 6(8): 597–603, doi: 10.1080/2150704X.2015.1062158

Cai Lina, Yu Wan, Shao Weizeng, et al. 2019. Satellite observations of suspended sediment near Ningbo North Dyke, China. Advances in Space Research, 64(7): 1415–1422, doi: 10.1016/j.asr.2019.07.013

Cai Lina, Zhou Minrui, Liu Jianqiang, et al. 2020. HY-1C observations of the impacts of islands on suspended sediment distribution in Zhoushan coastal waters, China. Remote Sensing, 12(11): 1766, doi: 10.3390/rs12111766

Chen Changsheng, Beardsley R C, Cowles G. 2006. An unstructured grid, finite-volume coastal ocean model—FVCOM user manual. Cambridge: Massachusetts Institute of Technology

Chen Yongqin, Chen Xiaohong. 2008. Modeling transport and distribution of suspended sediments in Pearl River Estuary. Journal of Coastal Research, 2008(10052): 163–170, doi: 10.2112/1551-5036-52.sp1.163

Chen Shenliang, Gu Guochuan. 2000. Modeling suspended sediment concentrations in the mouth of Hangzhou Bay. Journal of Sediment Research, (5): 45–50, doi: 10.3321/j.issn:0468-155X.2000.05.008

Chen Xiaoying, Zhang Jie, Tong Cheng, et al. 2019. Retrieval algorithm of chlorophyll-*a* concentration in turbid waters from satellite HY-1C coastal zone imager data. Journal of Coastal Research, 90(S1): 146–155, doi: 10.2112/SI90-018.1

Chen Yuxiang, Zuo Juncheng, Zou Huazhi, et al. 2016. Responses of estuarine salinity and transport processes to sea level rise in the Zhujiang (Pearl River) Estuary. Acta Oceanologica Sinica, 35(5): 38–48, doi: 10.1007/s13131-016-0857-2

Dai S, Yang Shilun, Cai A. 2008. Impacts of dams on the sediment flux of the Pearl River, southern China. Catena, 76(1): 36–43, doi: 10.1016/j.catena.2008.08.004

Dai Zhijun, Yun Caixing, Han Zhen. 2006. Composition of satellite remote sensing and digital topography applied in port projects. The Ocean Engineering, 24(1): 115–121

Egbert G D, Bennett A F, Foreman M G G. 1994. TOPEX/POSEIDON tides estimated using a global inverse model. Journal of Geophysical Research: Oceans, 99(C12): 24821–24852, doi: 10.1029/94JC01894

Egbert G D, Erofeeva S Y. 2002. Efficient inverse modeling of Baro-

tropic Ocean tides. Journal of Atmospheric and Oceanic Technology, 19(2): 183–204, doi: 10.1175/1520-0426(2002)019<0183:EIMOBO>2.0.CO;2

Elias E P L, Van Der Spek A J F, Wang Z B, et al. 2012. Morphodynamic development and sediment budget of the Dutch Wadden Sea over the last century. Netherlands Journal of Geosciences, 91(3): 293–310, doi: 10.1017/S0016774600000457

Feng Lian, Hu Chuanmin, Chen Xiaoling, et al. 2014. Influence of the three gorges dam on total suspended matters in the Yangtze Estuary and its adjacent coastal waters: observations from MODIS. Remote Sensing of Environment, 140: 779–788, doi: 10.1016/j.rse.2013.10.002

Forget P, Broche P, Naudin J J. 2001. Reflectance sensitivity to solid suspended sediment stratification in coastal water and inversion. Remote Sensing of Environment, 77(1): 92–103, doi: 10.1016/S0034-4257(01)00197-3

Gordon H R, Morel A Y. 1983. Remote Assessment of Ocean Color for Interpretation of Satellite Visible Imagery: A Review. New York: Springer

Graber H C, Beardsley R C, Grant W D. 1989. Storm-generated surface waves and sediment resuspension in the East China and Yellow seas. Journal of Physical Oceanography, 19(8): 1039–1059, doi: 10.1175/1520-0485(1989)019<1039:SGSWAS>2.0.CO;2

Huang Shuyi, Liu Jianqiang, Cai Lina, et al. 2020. Satellites HY-1C and Landsat 8 combined to observe the influence of bridge on sea surface temperature and suspended sediment concentration in Hangzhou Bay, China. Water, 12(9): 2595, doi: 10.3390/w12092595

Li Yangdong, Li Chunyan, Li Xiaofeng. 2017. Remote sensing studies of suspended sediment concentration variations in a coastal bay during the passages of atmospheric cold fronts. IEEE Journal of Selected Topics in Applied Earth Observations and Remote Sensing, 10(6): 2608–2622, doi: 10.1109/JSTARS.2017.2655421

Li Xiangdong, Shen Zhengguo, Wai O W H, et al. 2001. Chemical forms of Pb, Zn and Cu in the sediment profiles of the Pearl River Estuary. Marine Pollution Bulletin, 42(3): 215–223, doi: 10.1016/S0025-326X(00)00145-4

Li Xiangdong, Wai O W H, Li Y S, et al. 2000. Heavy metal distribution in sediment profiles of the Pearl River Estuary, South China. Applied Geochemistry, 15(5): 567–581, doi: 10.1016/S0883-2927(99)00072-4

Liu Guangping, Cai Shuqun. 2019. Modeling of suspended sediment by coupled wave-current model in the Zhujiang (Pearl) River Estuary. Acta Oceanologica Sinica, 38(7): 22–35, doi: 10.1007/s13131-019-1455-3

Lodhi M A, Rundquist D C, Han Luoheng, et al. 1998. Estimation of suspended sediment concentration in water using integrated surface reflectance. Geocarto International, 13(2): 11–15, doi: 10.1080/10106049809354637

Loisel H, Mangin A, Vantrepotte V, et al. 2014. Variability of suspended particulate matter concentration in coastal waters under the Mekong's influence from ocean color (MERIS) remote sensing over the last decade. Remote Sensing of Environment, 150: 218–230, doi: 10.1016/j.rse.2014.05.006

Montanher O C, Novo E M L M, Barbosa C C F, et al. 2014. Empirical models for estimating the suspended sediment concentration in Amazonian white water rivers using Landsat 5/TM. International Journal of Applied Earth Observation and Geoinformation, 29: 67–77, doi: 10.1016/j.jag.2014.01.001

Nanu L, Robertson C. 1990. Estimating suspended sediment concentrations from spectral reflectance data. International Journal of Remote Sensing, 11(5): 913–920, doi: 10.1080/01431169008955065

Novo E M L M, Steffen C A, Braga C Z F. 1991. Results of a laboratory experiment relating spectral reflectance to total suspended solids. Remote Sensing of Environment, 36(1): 67–72, doi: 10.1016/0034-4257(91)90031-Z

Park J W, Park S S. 1998. Hydrodynamic modeling of tidal changes due to land reclamation in an open-ended harbor, Pusan, Korea. Journal of Environmental Science and Health, Part A, 33(5): 877–890

Pope R M, Fry E S. 1997. Absorption spectrum (380–700 nm) of pure water. II. Integrating cavity measurements. Applied Optics, 36(33): 8710–8723, doi: 10.1364/AO.36.008710

Qiao Shuna, Pan Delu, He Xianqiang, et al. 2011. Numerical study of the influence of Donghai bridge on sediment transport in the mouth of Hangzhou Bay. Procedia Environmental Sciences, 10: 408–413, doi: 10.1016/j.proenv.2011.09.067

Qiu Zhongfeng. 2013. A simple optical model to estimate suspended particulate matter in Yellow River Estuary. Optics Express, 21(23): 27891–27904, doi: 10.1364/OE.21.027891

Shi Zhen, Xu Jie, Huang Xiaoping, et al. 2017. Relationship between nutrients and plankton biomass in the turbidity maximum zone of the Pearl River Estuary. Journal of Environmental Sciences, 57: 72–84, doi: 10.1016/j.jes.2016.11.013

Umeda S, Yamazaki T, Yuhi M. 2010. An experimental study of scour process and sediment transport around a bridge pier with foundation. In: International Conference on Scour & Erosion. San Francisco: American Society of Civil Engineers

Wang Chongyang, Li Weijiao, Chen Shuisen, et al. 2018. The spatial and temporal variation of total suspended solid concentration in Pearl River Estuary during 1987–2015 based on remote sensing. Science of the Total Environment, 618: 1125–1138, doi: 10.1016/j.scitotenv.2017.09.196

Wong L A, Chen J C, Xue Huijie, et al. 2003. A model study of the circulation in the Pearl River Estuary (PRE) and its adjacent coastal waters: 1. Simulations and comparison with observations. Journal of Geophysical Research: Oceans, 108(C5): 3156, doi: 10.1029/2002JC001451

Wu Guofeng, Cui Lijuan, Duan Hongtao, et al. 2013. An approach for developing Landsat-5 TM-based retrieval models of suspended particulate matter concentration with the assistance of MODIS. ISPRS Journal of Photogrammetry and Remote Sensing, 85: 84–92, doi: 10.1016/j.isprsjprs.2013.08.009

Wu Chuangshou, Yang Shilun, Huang Shichang, et al. 2014. Multiscale variability of water discharge and sediment load in the Pearl River during 1954–2011. Acta Geographica Sinica, 69(3): 422–432

Xia Xiaoming, Li Yan, Yang Hui, et al. 2004. Observations on the size and settling velocity distributions of suspended sediment in the Pearl River Estuary, China. Continental Shelf Research, 24(16): 1809–1826, doi: 10.1016/j.csr.2004.06.009

Xu F L, Lam K C, Zhao Z Y, et al. 2004. Marine coastal ecosystem health assessment: a case study of the Tolo Harbour, Hong Kong, China. Ecological Modelling, 173(4): 355–370, doi: 10.1016/j.ecolmodel.2003.07.010

Yan Huakun, Wang Nuo, Yu Tiaolan, et al. 2015. Hydrodynamic behavior and the effects of water pollution from Dalian's large-scale offshore airport island in Jinzhou Bay, China. Journal of Waterway, Port, Coastal, and Ocean Engineering, 141(1): 05014003

Yang Feng, Shen Xiaohua, Zou Lejun. 2003. Application of fitting method of nonlinear equations to quantitative models of remote sensing data and suspended solids. Remote Sensing Technology and Application, 18(3): 138–143, doi: 10.3969/j.issn.1004-0323.2003.03.004

Yang Qian, Stramski D, He Mingxia. 2013. Modeling the effects of near-surface plumes of suspended particulate matter on remote-sensing reflectance of coastal waters. Applied Optics, 52(3): 359–374, doi: 10.1364/AO.52.000359

Yanmaz A M, Altinbilek H D. 1991. Study of time-Dependent local scour around bridge piers. Journal of Hydraulic Engineering, 117(10): 1247–1268, doi: 10.1061/(ASCE)0733-9429(1991)117:10(1247)

Yuan Xingzhong, Lu Jianjian. 2001. Influence of diking on the benthic macro-invertebrate community structure and diversity in the south bank of the Changjiang Estuary. Acta Ecologica Sinica, 21(10): 1642–1647, doi: 10.3321/j.issn:1000-0933.2001.10.012

Yuan Zhongzhi, Shao Jing'an, Chen Xiaoling. 2009. Spatio-temporal analysis of the suspended sediment concentration in the Pearl

River Estuary and Shenzhen Bay based on the information analysis theory. Resources Science, 31(8): 1415–1421

Zhang Minwei, Dong Qing, Cui Tingwei, et al. 2014. Suspended sediment monitoring and assessment for Yellow River Estuary from Landsat TM and ETM + imagery. Remote Sensing of Environment, 146: 136–147, doi: 10.1016/j.rse.2013.09.033

Zhang Minwei, Tang Junwu, Dong Qing, et al. 2010. Retrieval of total suspended matter concentration in the Yellow and East China seas from MODIS imagery. Remote Sensing of Environment, 114(2): 392–403, doi: 10.1016/j.rse.2009.09.016

Zhao Ke, Qiao Lulu, Shi Jinghao, et al. 2015. Evolution of sedimentary dynamic environment in the western Jiaozhou Bay, Qingdao, China in the last 30 years. Estuarine, Coastal and Shelf Science, 163: 244–253

Zhu Fan, Ou Suying, Zhang Shuohan, et al. 2015. MODIS images-based retrieval and analysis of spatial-temporal change of superficial suspended sediment concentration in the Pearl River Estuary. Journal of Sediment Research, (2): 67–73

Zu Tingting, Wang Dongxiao, Gan Jianping, et al. 2014. On the role of wind and tide in generating variability of Pearl River plume during summer in a coupled wide estuary and shelf system. Journal of Marine Systems, 136: 65–79, doi: 10.1016/j.jmarsys.2014.03.005